Characterization and Synthesis of α-Fe2O3 Nanoparticles and α-Fe2O3 /CuO Nanocomposite by hydrothermal method and application them in a solar cell

Ghanem Abdulnabi
Chemistry Department, Faculty of Science, Kufa University, Najaf, Iraq,
ghanemn.alkreete@student.uokufa.edu.iq

Amer Musa Juda
Chemistry Department, Faculty of Science, Kufa University, Najaf, Iraq.

Abstract

CuO and α-Fe2O3 metal oxide nanostructures were prepared using the hydrothermal technique. In addition, α-Fe2O3/CuO nanocomposites were generated using the hydrothermal method by fusing them in equal amounts. Transmission electron microscopy (TEM), X-ray diffraction and field emission scanning electron microscopy were used to evaluate the properties of the produced composites (FE-SEM). , respectively, according to the images from FE-SEM, and the α-Fe2O3/CuO nanocomposites organized as (cube). The X-ray diffraction results indicated the presence of CuO and α-Fe2O3 a (monoclinic, hexagonal structure), respectively. with average crystal sizes (18.03, 14.55 and 23.22) nm for CuO, α-Fe2O3 and α-Fe2O3/CuO, respectively. The optical properties of the prepared compounds were studied through visible and ultraviolet spectroscopy. The optical band gap is (2.1, 1.6 and 1.8) eV for CuO, α-Fe2O3 NPs and α-Fe2O3/CuO nanocomposites. Dye-sensitized solar cells (DSSCs) fabricated based on CuO, α-Fe2O3 NPs and α-α-Fe2O3/CuO were cast on a perfluorinated tin oxide front electrode. While the FTO carbon/glass substrate serves as the back electrode. Iodine/iodide KI/I2 was used as the electrolyte solution, and the natural green dye was used. The solar cell efficiencies of CuO, α-Fe2O3Nps, α-Fe2O3/CuO nanocomposites of CuO and α-Fe2O3/CuO nanocomposites/dye-leek green were (1.51, 1.7and 1.56), respectively.

Keywords: *Nanocomposite, Hydrothermal, DSSCs.*

1. INTRODUCTION

The foundation of nanoscience and nanotechnology is nanomaterials. Over the past few years, research and development activity in the vast and interdisciplinary field of nanostructure science and technology has exploded globally. It includes The variety and kind of functions that may be accessible, as well as the processes used to generate materials and products, which have the potential to revolutionize. It already has a large commercial influence, and that impact will undoubtedly grow in the future[1]. A wide range of various substances is used to create semiconductor nanocrystals (NCs). Based on the periodic table, they are referred to as II-VI, III-V, or IV-VI semiconductor nanocrystals. groups that these components are formed into. GaN, GaP, GaAs, InP, and In As, for instance, are III-V semiconductors, while ZnO, ZnS, CdS, CdSe, and CdTe are II-VI semiconductors[2]. Iron oxide is a transition metal oxide that comes in a wide range of stoichiometric and crystalline forms, including magnetite (Fe3O4), maghemite (-

Fe2O3), hematite (-Fe2O3), barite, and maghemite wüstite (FeO). Due to its narrow bandgap, hematite (Fe2O3) has demonstrated the highest stability under ambient settings. (2.0–2.2 eV). Six oxygen atoms surround the iron atoms in a hematite crystal (hexagonal)[3]. Recently, interest in semiconductor-based nanocomposites has increased in several scientific and technological fields. Among semiconductor materials, CuO and its composites have become a strong contenders in the field of photocatalysis. Its physical and chemical characteristics include stable, abundant, harmless, and affordable. It also has a narrow band gap energy of 1.2–1.6 eV[4]. The term "hydrothermal synthesis" refers to heterogeneous processes that take place in aqueous environments at temperatures and pressures above ambient in this instance, a reaction autoclave's pressure is significantly raised over atmospheric pressure by heating an aqueous combination of precursors in a sealed stainless steel autoclave [5]. Ultrafine grain size, regulated particle morphology, uniform content, excellent purity, and the avoidance of the calcination stage are all characteristics of the hydrothermal synthesis process[6]. Utilizing solar energy may enhance our quality of life, lessen our reliance on other energy sources such as fossil fuels, and boost our economy by adding new jobs. Solar cells, also known as photovoltaic cells, are among the most effective and promising sources of renewable energy. These resources include solar thermal energy, wind energy (air), gravitational potential energy (water or hydroelectric energy), tidal energy, and biomass energy. The Michael Gratzel-invented dye-sensitized solar cell (DSSC), one of several types of solar cells, was created in 1991[7]. A DSSC typically has a "sandwich" architecture because it primarily consists of four sections, as seen in Figure 1: Light-sensitizing dye (dye molecules are linked with the semiconductor to the photoanode); photoanode (semiconductor oxide placed on a transparent substrate); electrolyte (redox couple); and counter electrode (generally, a thin film of platinum or carbon graphite). The basic working concept of a cell is the dye's ability to absorb photons from solar radiation. Due to the fact that the sun's radiative power is higher in the visible area of the electromagnetic spectrum, the sensitizing molecule must have a strong absorption in this region. The dye is then activated by promoting an electron onto the photoelectrode, which is typically nanostructured TiO2[8].

Figure 1. typical DSSC elements and working procedures[8].

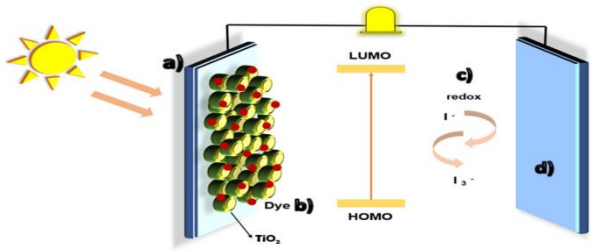

2. Materials and Method

2-1. Materials and devices

The properties of the prepared compounds are investigated through Field Emission Scanning Electron Microscopy (FE-SEM) type (TESCAN BRNO-Mira3LMU/ Tescan), Transmission Electron Microscopy (TEM)) type (Philips em 208s,100Kv)and X-Ray Diffraction (XRD) type (6000/Shimadzu, Japan). All chemicals in this work were purchased from Merck company and used without further purification such as NaOH (98%), CuSO4.5H2O(98%) and FeCl3.6H20 (97%). The efficiency of the solar cell was calculated by a Programmable Keithley electrometer (2400, Tektronix Company) with the relation.

2-2.Synthesis of α-Fe2O3 Nanoparticles and α-Fe2O3 /CuO Nanocomposite.

2-2-1. Synthesis of α-Fe2O3 Nanoparticles

The hydrothermal method is abundantly used for synthesizing metal oxide nanostructures the current study, hydrothermal preparation was used to create -Fe2O3 nanoparticles. Initially, 100 ml of deoxygenated distilled water was used to dissolve 4.052 g of iron (III) chloride hexahydrate (FeCl3, 6H2O) under magnetic stirring for 30 min at 80 ℃. Ammonia in 50 ml added hydroxide (NH4OH) to keep the pH at 11. The solution was put into a Teflon-lined autoclave made of stainless steel, where it was hydrothermally treated for 12 hours at 160 ℃. The precipitate that resulted from this was separated by centrifugation at 6000 rpm, washed repeatedly with distilled water and ethanol, and then dried in the air at 80 ℃ and calcined for four hours at 700 ℃ [9].

2-2-2. Synthesis of α-Fe2O3 /CuO Nanocomposite

The hydrothermal method was used for α-Fe2O3 /CuO synthesis .2. 26 g of FeCl3 and 2.0 g of CuSO4 .5H2O were dissolved in 100 mL of distilled water and 0.8 M of NaOH were added to the solution medium until the pH 8, and the stirring continued until a homogeneous solution was obtained. Then, the solution was transferred to the Teflon autoclave reactor and kept in the oven for 20 hours at 140C°. The sample was filtered and rinsed with distilled water and then ethanol multiple times before being dried in a vacuum at 60 C0 for 4 hours after the autoclave had naturally cooled to the room. Then, the solution was transferred to the Teflon autoclave reactor and kept in the oven for 20 hours at 150C°.The. After the autoclave had naturally cooled to room temperature, the sample was filtered and washed with distilled water and then ethanol several times before being dried in a vacuum at 50 Co for 5 hours[10].

3. RESULTS AND DISCUSSIONS

3-1.X-ray diffraction analysis

Figure (2) shows the XRD peaks of CuO NPs at 100 Co (PH=10) nanoparticles appeared at 33.11°,36.23 °,38.94°,54.36°,60.24°,61.24°and 68.34° corresponding to (101), (004), (200), (105), (211), (204),(220) and (215). respectively, which indicates the formation of a monoclinic structure (CuO) crystal structure with space group (C2/c), monoclinic structure, conforms to the monoclinic structure (JCPDS No. 80-1268) with average crystalline size (8.6) nm[11]. Figure (3) shows the XRD peaks of (α-Fe2O3) NPs appeared at 61.24°,68.34°,26.25°,33.24°, 36.31°,39.44°,49.84°,54.26°and 63.04° corresponding to(102), (104), (105), (017), (110), (113), (207), (201), and (300). respectively, which indicates the (α-Fe2O3)structure is hexagonal with the space group (P1) This finding is consistent with the standard (JCPD 40-1139) data .with an average crystalline size (13.10)nm. The peaks then become sharper and more intense with the of (α-Fe2O3) at 400 ° C for three hours[11]. Figure (3) displays the XRD patterns obtained from samples α-Fe2O3/ CuO nanocomposite. Sample α-Fe2O3/ CuO XRD diffraction peaks in Figure (4) are consistent with the expected (102), (0012), (204), and (2010) reflections of the hexagonal (H) iron oxide phase, α-Fe2O3 (Hematite) (JCPD file number: 040-1139). Rhombohedral (R) structure α-Fe2O3 is also reflected in the (101), (104), (113), (200), (116), (122), and (214), planes (JCPD file number:001-1053). The usual peaks of (-111) and (004) reflections of CuO are found at 2 values of 35.28° and 74.34° in sample α-Fe2O3/ CuO, with d-values and intensities that are consistent with those of the reported very strong peak (JCPD file number: 5-661) [12].

Figure (2): XRD patterns CuO NPs at 100 oC prepared by hydrothermal method

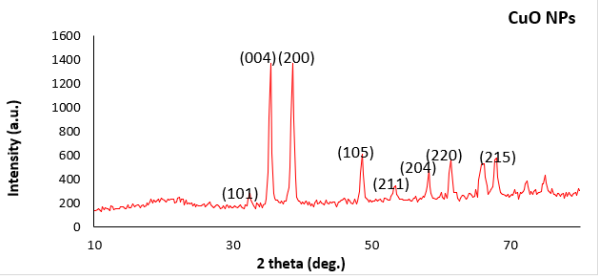

Figure (3): XRD patterns of α-Fe2O3 NPs prepared by hydrothermal method.

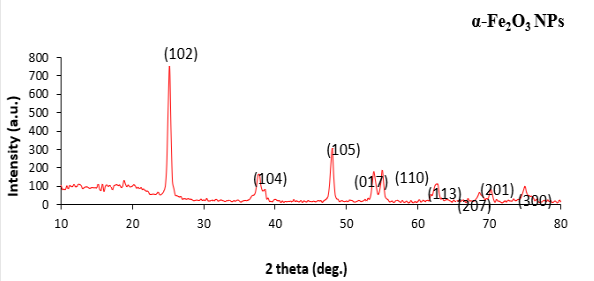

Figure 4. XRD patterns of α-Fe2O3/ CuO nanocomposite at 400 C0 for 3 h.

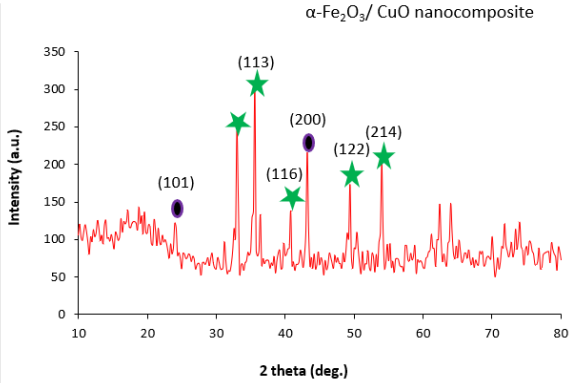

3-2.FESEM Analysis of CuO, , α-Fe2O3 and (α-Fe2O3 /CuO) Nanocomposites

The particle size and shape are (40.69 to 60.67) nm and the spherical-like structure of CuO NPs at 100 C for 2h at (PH=10) by the hydrothermal method, as shown in figure (3) (A-D). The effect of temperature was found on the synthesis of CuO nanostructures, this is because the crystalline nature of CuO increased with increasing the temperature of the reaction n to 100 °C, as shown in XRD results [13]. The particle size and shape are (33 to 48) nm and the plate-structure of α-Fe2O3 NPs at 400 oC for 3h at PH=10 by the hydrothermal method, as shown in Figure(4) [14]. Figure 5 shows the FE-SEM images of the α-Fe2O3/CuO nanocomposite prepared by the hydrothermal method. In figure 3. (a), zones of α-Fe2O3/ CuO were marked to show the contrast, they contain cracks formed as a result of the surface tension in the condensation step. In the lower zone, the clusters back are covered with a nanocomposite of α-Fe2O3/ CuO. The particle size was about (24to 557 nm), and the shape is cubic that consists of an aggregation of particles with 25 nm of the average size [14].

Figure 5. FE-SEM images of CuO NPs prepared by hydrothermal method at 100 C0 for 2h at pH=10.

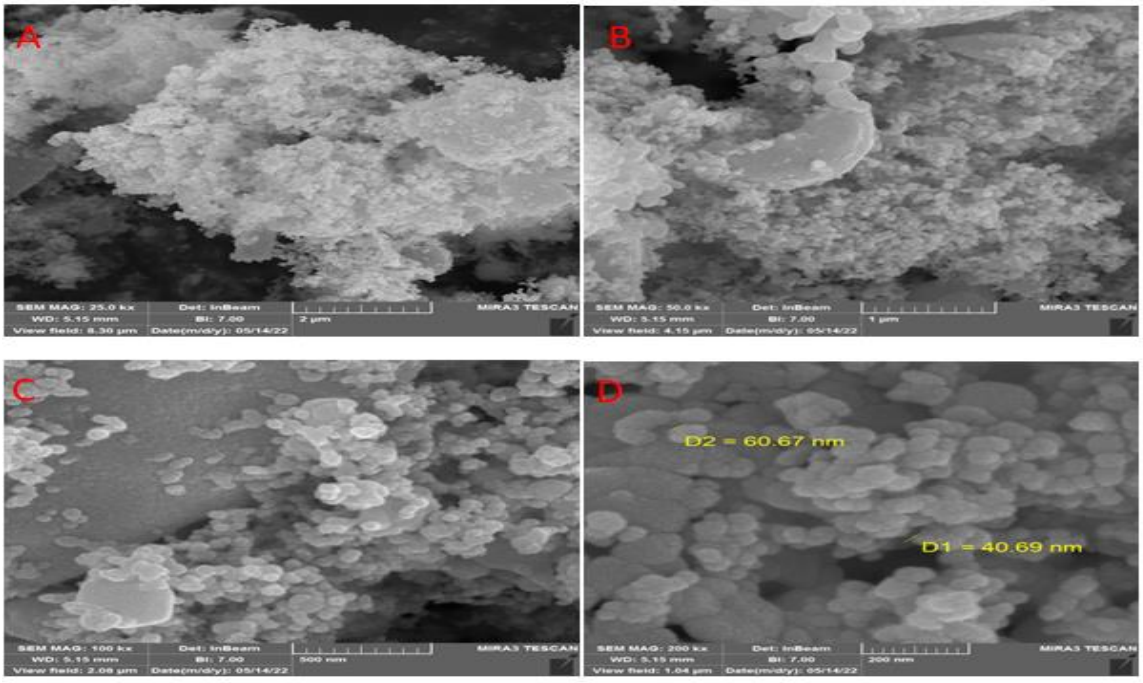

Figure 6. FE-SEM images of α-Fe2O3 NPs prepared by hydrothermal method

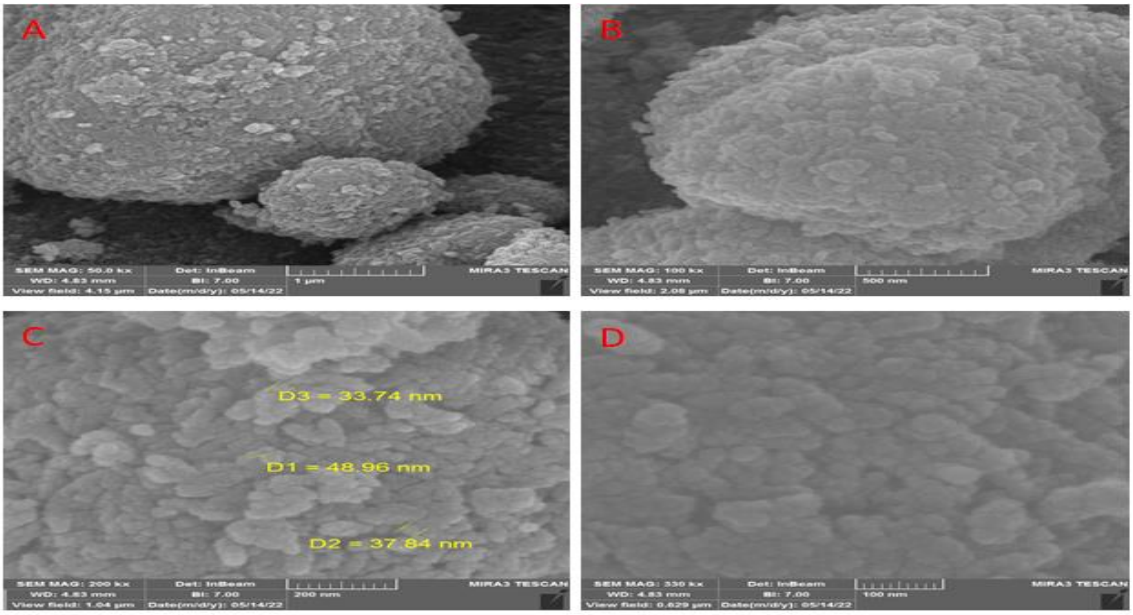

Figure 7. FE-SEM images of α-Fe2O3/ CuO nanocomposite prepared by hydrothermal method at 400 C0 for 3h.

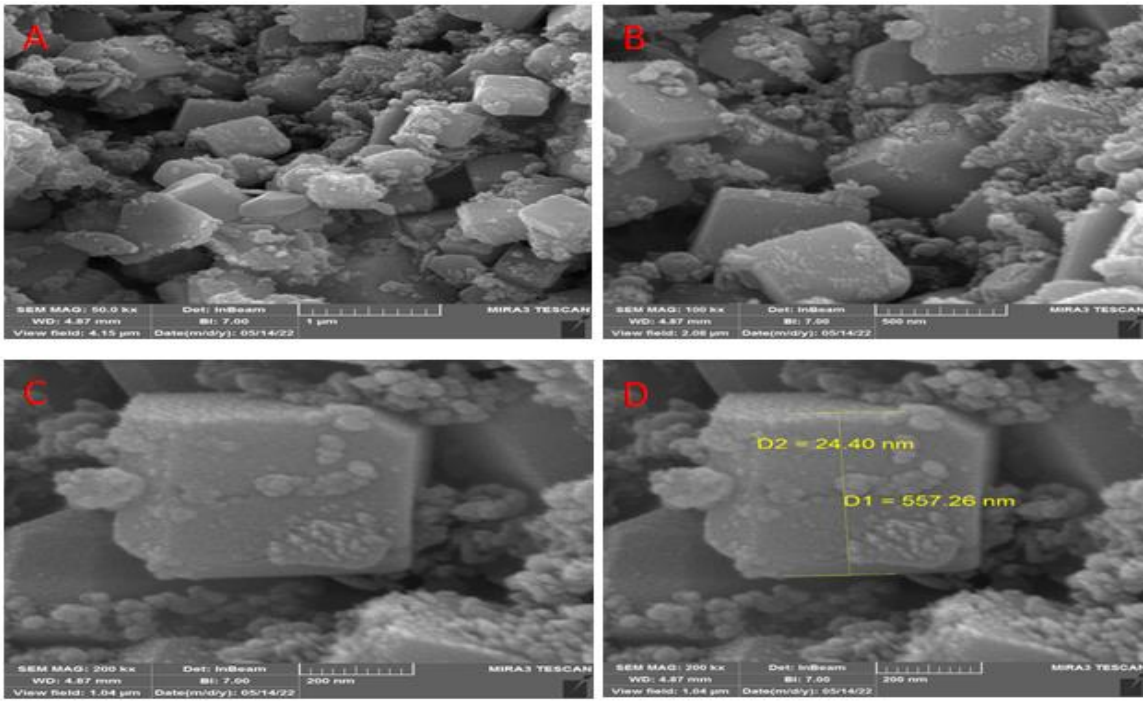

3-3.TEM Analysis of CuO,TiO2, α-Fe2O3 and (CuO /TiO2/ α-Fe2O3) Nanocomposites

TEM images of copper oxide nanoparticles (CuO) NPs were prepared by using the hydrothermal method at 100 oC for 2h at PH=10, as shown in Figure 8 (A-D), where the microscopic images confirm the formation of spherical nanoparticles since the fission process took place in a free medium without any capping factor, some particles were overlapping among themselves, as it was noted that Some spherical nanoparticles appear in small size due to the phenomenon of agglomeration. The average size of copper oxide nanoparticles was (25 to 50 nm). [15]. Transmission electron microscopy is used to analyze the morphology and average grain size of pure α-Fe2O3 NPs, as shown in Figure 9 (A-D). The formation and growth of NPs provide the basis for this trend. NPs with small diameters can be developed thanks to a longer reaction time. There is some agreement between the size of the produced IONPs and the size described in the literature on solvent-less synthesis of IONPs by the Hydrothermal technique. Changes in PH cause a decrease in the size of α-Fe2O3 NPs, from 15 to 20 nm with Nanorod nanoparticles. In this case, the longer the heating period, the smaller the NPs will be [16]. As shown in Figure 10 (A-D), CuO/α-Fe2O3 nanocomposite prepared by the hydrothermal method has an average grain size of 30–50 nm. In addition, a small amount of cube-like crystals appeared. From Figure 10 (A-D), one can see that the sample with a CuO/α-Fe2O3 nanocomposite ratio of (1:1) was composed of uniform nanoparticles with a mean size of around 30 nm [17].

Figure 8. TEM images of CuO NPs prepared by hydrothermal method

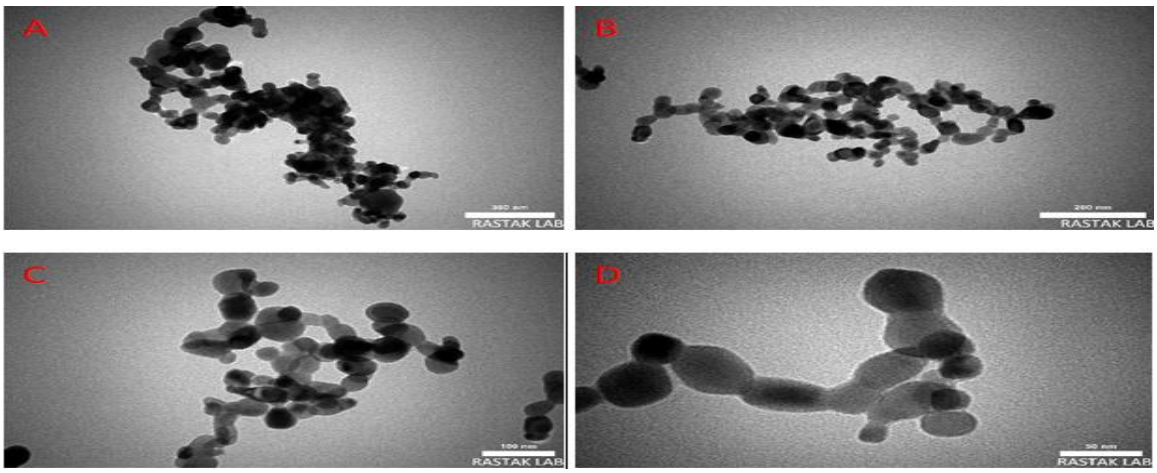

Figure 9. TEM images of α-Fe2O3 NPs prepared by hydrothermal method

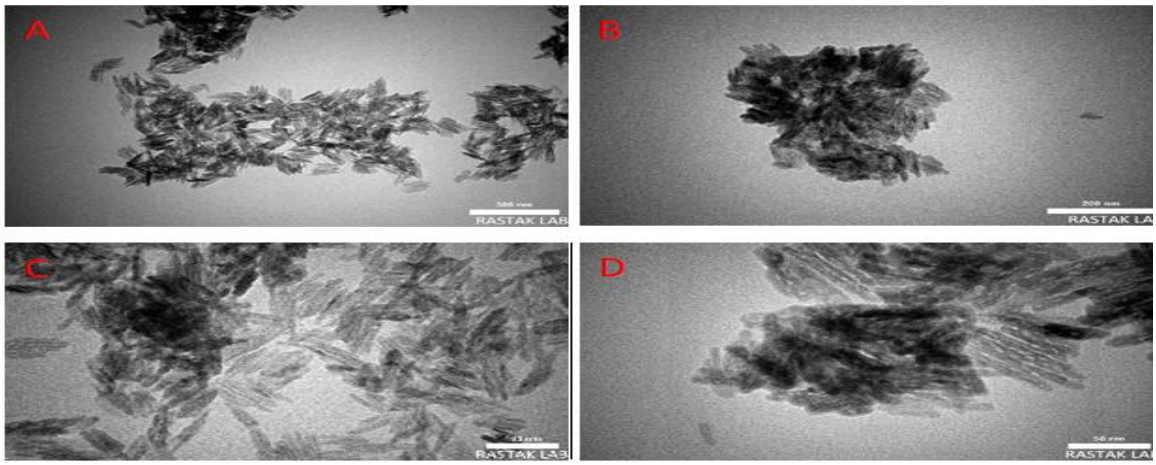

Figure 10. TEM images of CuO/α-Fe2O3 nanocomposite prepared by hydrothermal method

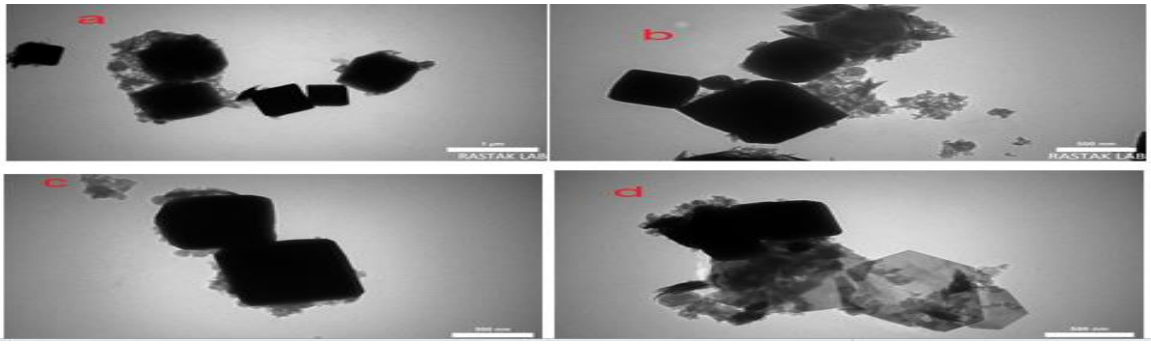

3-4.Optical Properties

The efficiency of the solar cell was calculated by a Programmable Keithley electrometer (2400, Tektronix Company) with the relation.

FF=JMAX *VMAX/JSC* VOC (1)

where: JSC is the short circuit current, VOC is the open-circuit voltage

, JMAX is the maximum current, VMAX is the maximum voltage

The absorption spectra and energy band gap of CuO, α-Fe2O3, nanoparticles and α-Fe2O3/CuO nanocomposites are shown in Figures(11, 12, 13,) and Table 1.

Table 1. shows the energy band gap of CuO, α-Fe2O3, and α-Fe2O3/CuO

CuO	2.1 ev
α-Fe_2O_3	1.6ev
α-Fe2O3/ CuO	1.8ev

Figure.11: The absorbance spectrum and optical band gap of CuO nanoparticles.

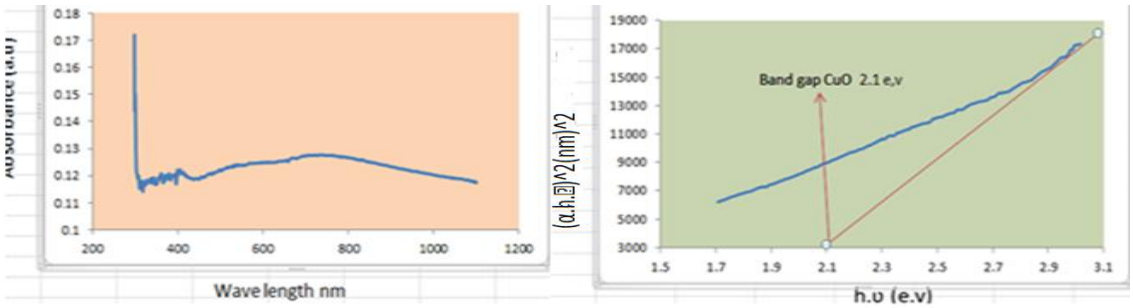

Figure.12: The absorbance spectrum and optical band gap of α-Fe2O3 nanoparticles.

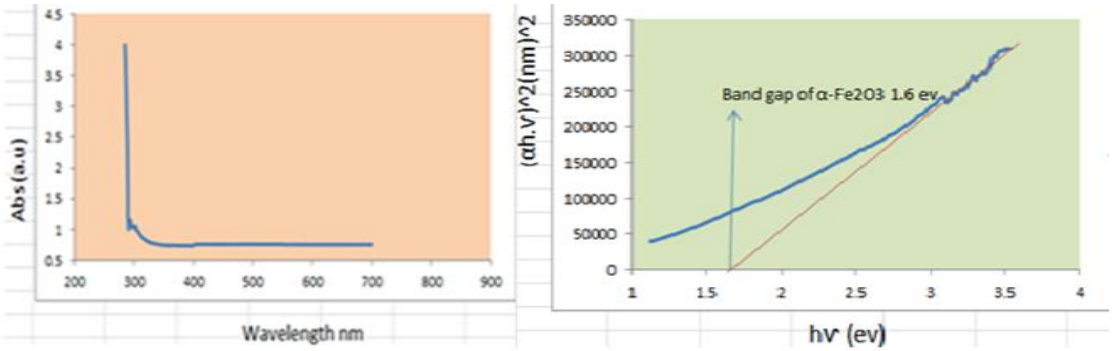

Figure13. The optical band gap and absorbance spectrum of CuO/ α-Fe2O3 nanoparticles

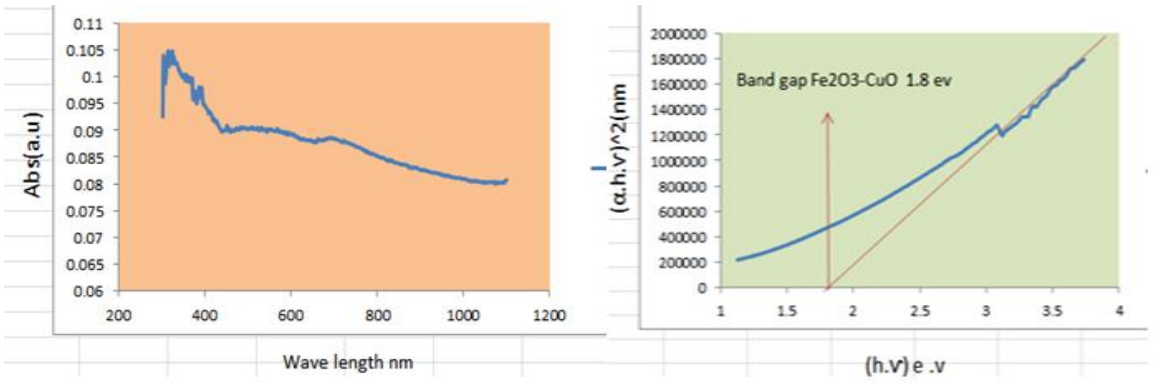

3-5.The Applications.

3.5-1.Fabrication of Dye-Sensitized Solar Cells.

DSSCs are fabricated by using CuO, α-Fe2O3 nanoparticles and α-Fe2O3/ CuO nanocomposites as photoelectrode and natural dye green leek dye was used as an absorbent medium. Figures14.(A, B, C,) shows the I-V

characteristics of DSSCs prepared based on α-Fe2O3, CuO NPS and α-Fe2O3 /CuO nanocomposites / green leek dye has given VOC, ISC and efficiency (η%) are shown in a Table(2).

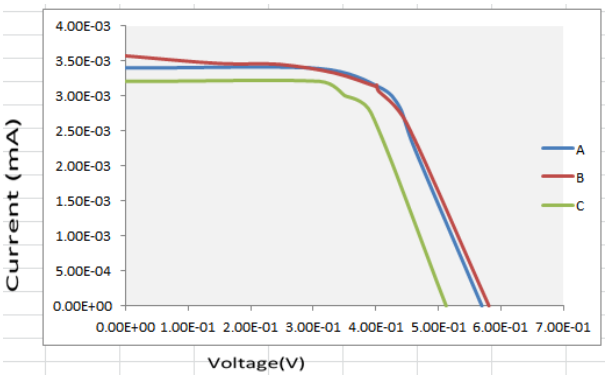

Figure14. I-V characteristics of prepared DSSCs, (A) α-Fe2O3 /CuO(B) α-Fe2O3, and (C) CuO green leek dye.

Table.2.Photo electrochemical parameters of the DSSCs, A=0.25cm2 under intensity light28.2 Mw/cm 2 using/ green leek dye.

Catalyst/ green leek dye	I_{SC} Ma	V_{OC} (V)	Imax mA	Vmax (V)	Pmax	FF%	η%
α-Fe_2O_3	3.57	0.594	2.58	0.424	1.09	0.51	1.7
CuO	4.10	0.498	3.08	0.314	0.961	0.47	1.51
α-Fe_2O_3/CuO	3.59	0.502	2.91	0.348	1.00	0.55	61.5

The results show that the efficiency of DSSC made based on α-Fe2O3 with shallot green dye is higher than that of CuO, α-Fe2O3 NPs and α-Fe2O3/CuOnanocomposites. Because it has a low energy gap (1.6 ev). Efficiency rises when energy gaps narrow. This is because narrow energy bandgaps make it possible for electrons with lower excitation energy to become free electrons in the conduction band which increases the efficiency of solar energy production. [18].The second of α-Fe2O3 has an area of 74.604m2/g which is higher than that of CuO NPs and α-Fe2O3/CuO nanocomposites. This indicates that more dye can adsorb onto the surface of α-Fe2O3, which may enhance the efficiency of the fabricated DSSC[19]. Moreover, the low value obtained from the fabricated DSSCs is also due to the low intensity (28.2 mW/cm2) of the light source used.

4. Conclusions

CuO, α-Fe2O3 and α-Fe2O3/CuO nanoparticles were prepared by a simple and safe hydrothermal method. Deposition of semiconductor on FTO glass by doctor blade gives a better homogeneous surface than dropping and evaporation of semiconductor solution suspended on FTO. Several techniques have been used to characterize the treated products using X-ray diffraction, transmission electron microscopy (TEM), and field emission scanning electron microscopy (FE-SEM) (XRD). It is noted from the previous data that the dye has a very important role in improving the efficiency of the solar cell. The results showed that cells prepared from α-Fe2O3 NPs have better efficiency than CuO NPs and α-Fe2O3/CuO nanocomposites.

Reference

1. Alagarasi, A., Chapter-introduction to nanomaterials. 2011, Go to reference in article.
2. Sahu, M.K., Semiconductor nanoparticles theory and applications. Int. J. Appl. Eng. Res, 2019. 14(2): p. 491-494.
3. Cherepy, N.J., et al., Ultrafast studies of photoexcited electron dynamics in γ-and α-Fe2O3 semiconductor nanoparticles. The Journal of Physical Chemistry B, 1998. 102(5): p. 770-776.

4. Azharudeen, A.M., et al., Solar Power Light-Driven Improved Photocatalytic Action of Mg-Doped CuO Nanomaterial Modified with Polyvinylalcohol. Journal of Nanomaterials, 2022. 2022: p. 2430840.
5. Lothenbach, B., et al., Solubility and characterization of synthesized 11 Å Al-tobermorite. Cement and Concrete Research, 2022. 159: p. 106871.
6. Hu, W., et al., W–Y2O3 composite nanopowders prepared by hydrothermal synthesis method: Co-deposition mechanism and low temperature sintering characteristics. Journal of Alloys and Compounds, 2020. 821: p. 153461.
7. Agrawal, A., et al., Advancements, frontiers and analysis of metal oxide semiconductor, dye, electrolyte and counter electrode of dye sensitized solar cell. Solar Energy, 2022. 233: p. 378-407.
8. Castillo-Robles, J.A., et al., Advances on Dye-Sensitized Solar Cells (DSSCs) Nanostructures and Natural Colorants: A Review. Journal of Composites Science, 2021. 5(11): p. 288.
9. Lassoued, A., et al., Synthesis, photoluminescence and Magnetic properties of iron oxide (α-Fe2O3) nanoparticles through precipitation or hydrothermal methods. Physica E: Low-dimensional Systems and Nanostructures, 2018. 101: p. 212-219.
10. Kunya, S.I., M.K.M. Yunusa Abdu, and M.K. Ahmad, PROPOSAL FOR HYDROTHERMAL TECHNIQUE FOR METAL OXIDE NANOMATERIAL SYNTHESIS: THE CASE OF ZnO AND TiO2. 2022.
11. Padil, V.V.T. and M. Černík, Green synthesis of copper oxide nanoparticles using gum karaya as a biotemplate and their antibacterial application. International journal of nanomedicine, 2013. 8: p. 889.
12. Maji, S.K., et al., Synthesis, characterization and photocatalytic activity of α-Fe2O3 nanoparticles. Polyhedron, 2012. 33(1): p. 145-149.
13. Abid, M.A., et al., Iron oxide nanoparticles synthesized using garlic and onion peel extracts rapidly degrade methylene blue dye. Physica B: Condensed Matter, 2021. 622: p. 413277.
14. Tamuly, C., et al., Reduction of aromatic nitro compounds catalyzed by biogenic CuO nanoparticles. RSC Advances, 2014. 4(95): p. 53229-53236.
15. Bhosale, M.A., et al., Magnetically separable γ-Fe2O3 nanoparticles: An efficient catalyst for acylation of alcohols, phenols, and amines using sonication energy under solvent free condition. Journal of Molecular Catalysis A: Chemical, 2015. 404: p. 8-17.
16. Pan, L., J. Tang, and F. Wang, Facile synthesis of nanoscaled α-Fe2O3, CuO and CuO/Fe2O3 hybrid oxides and their electrocatalytic and photocatalytic properties. Open Chemistry, 2013. 11(5): p. 763-773.
17. Bootluck, W., et al., Modification of surface α-Fe2O3/TiO2 photocatalyst nanocomposite with enhanced photocatalytic activity by Ar gas plasma treatment for hydrogen evolution. Journal of Environmental Chemical Engineering, 2021. 9(4): p. 105660.
18. Elhouri, S.A., The Value of Efficiency and Energy Gap for Different Dye Solar Cells. Global Journal of Engineering Science and Researches, 2018. 5(8): p. 115-121.

19. Son, Y.J., et al., Influence of TiO2 particle size on dye-sensitized solar cells employing an organic sensitizer and a cobalt (III/II) redox electrolyte. The Journal of Physical Chemistry C, 2018. 122(13): p. 7051-7060.